ORGANIC CHEMISTRY FRONTIERS

RESEARCH ARTICLE

View Article Online
View Journal | View Issue

Cite this: *Org. Chem. Front.*, 2019, **6**, 1257

Synthesis, photophysical properties, and self-dimerization studies of 2-λ^5-phosphaquinolin-2-ones†

Jeremy P. Bard, [a] Chun-Lin Deng, [a] Hannah C. Richardson, [b] Jacob M. Odulio,[a] Joshua E. Barker, [a] Lev N. Zakharov, [c] Paul H.-Y. Cheong, [b] Darren W. Johnson *[a] and Michael M. Haley *[a]

Received 4th February 2019,
Accepted 23rd March 2019

DOI: 10.1039/c9qo00199a

rsc.li/frontiers-organic

We have rationally designed and synthesized a library of phosphaquinolinone derivatives containing various electron-donating and -withdrawing groups on two positions of the scaffold. Distinct trends are observed between the substituents on R^1 and R^2 with both the photophysical properties of the molecules and their dimerization strengths. With withdrawing groups upon the scaffold, dimerization constants surpass 500 M^{-1} in H_2O-saturated $CDCl_3$. Computational studies on the dimeric structures corroborate the experimental findings.

Introduction

The coumarin (2*H*-1-benzopyran-2-one) scaffold[1–7] along with its aza-analogue carbostyril (2(1*H*)-quinolinone)[8–13] comprise a fascinating class of compounds. In addition to marked physiological activity,[14,15] the coumarin/carbostyril framework has been widely established as one of the most useful small molecule fluorophores (Fig. 1). With respectable Stokes shifts and quantum yields as well as good chemical stability, this scaffold and its derivatives have been the subject of a plethora of studies and applications.[16–18] The variety of derivatization for both molecules is impressive, as a multitude of substituents can be installed on the frameworks. Nonetheless, there are very few examples of modification of the base heterocyclic skeletons themselves, limiting the applications and functionalities to the lactone/lactam cores. Judicious modification of the backbone could afford a wealth of new derivatives whose improved and modified properties would allow for further applicability of these molecules.

One such modification could be replacement of the carbonyl moiety (C═O) with an isolobal P(OR)═O group to yield a "phosphaquinolinone". While such six-membered heterocycles containing adjacent phosphorus and nitrogen (PN) atoms have been known since 1960 (phosphinamidate **A**, phosphonamidate **B**),[19,20] their syntheses and isolation were often plagued by various challenges. More recent work has examined metal-mediated routes to phosphonamidates such as **C**.[21–25] A family of structurally related phosphinamides (*e.g.*, **D**) has also been investigated as a route to chiral phosphines.[26–29] Further, a similar five-membered phosphinamide system has recently been reported showing uniquely flexible dimerization

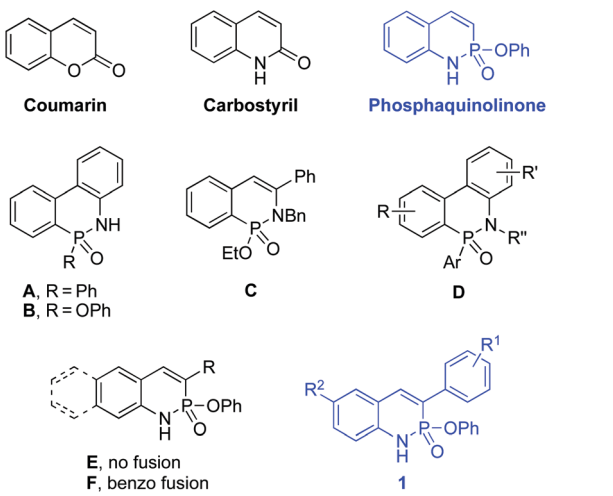

Fig. 1 Coumarin and two congeners, carbostyril and phosphaquinolinone, along with known phosphaquinolinones **A**–**F**.

[a]*Department of Chemistry & Biochemistry and the Materials Science Institute, University of Oregon, Eugene, Oregon 97403-1253, USA. E-mail: haley@uoregon.edu, dwj@uoregon.edu*
[b]*Department of Chemistry, Oregon State University, Corvallis, Oregon 97331, USA*
[c]*CAMCOR, University of Oregon, Eugene, Oregon 97403-1433, USA*

†Electronic supplementary information (ESI) available: Detailed experimental procedures for synthesis and characterization of new compounds, crystal data and packing, theoretical calculations, and copies of NMR spectra as a PDF file. CCDC 1894569–1894573. For ESI and crystallographic data in CIF or other electronic format see DOI: 10.1039/c9qo00199a

properties favourable for self-assembled soft materials.[30] Despite the recent revival in interest, structures that encompass such six-membered PN-heterocyclic motifs are rather uncommon.

To help address this issue, we recently reported a series of water- and air-stable phosphonamidates based on scaffold **E**.[31] Along with the benzo-fused analogues **F**,[32] this class of heterocycles is fluorescent, with electron withdrawing groups (EWGs) at R leading to a red-shifted emission and electron donating groups (EDGs) furnishing a blue-shifted emission. Additionally, the strong polarization of the oxygen in the hydrogen bond accepting P═O unit and the adjacent acidic N–H hydrogen bond donor lead to surprisingly strong dimerization between the (*R*)- and (*S*)- enantiomers (*meso*-dimer), potentially due to a minimization of repulsive secondary interactions. Though these properties are both intriguing and give promise for unique applications of this PN scaffold, a more detailed, systematic understanding of their fundamental structure–property relationships must be acquired first before any applications can be pursued. Herein we present the synthesis, optoelectronic properties, computational examination, and dimerization studies both in solution and in the solid state of a series of phosphaquinolinones based on phosphonamidate **1**.

We dedicate this manuscript to Prof. Julius Rebek, Jr. for his mentorship, friendship, and tremendous achievements in molecular recognition, self-replicating systems, tests for reactive intermediates, self-assembly, and hydrogen bonding, among many other areas. Therefore, we would be remiss not to point out that one of us (DWJ) learned of the strength of simple homo- and hetero-dimers of cyclic ureas, lactams, and cyclic sulfamides from, first, Rebek's report of a tetrameric hydrogen bonded capsule assembled through strong, complementary hydrogen bonds between cyclic ureas and sulfamides;[33] and, second, from Prof. Rebek's class on molecular recognition at The Scripps Research Institute.‡ In these studies, Rebek and coworkers discovered that heterodimers between simple model cyclic ureas and sulfamides were stronger than their homodimers.[33] Subsequent studies by Fraser Hof in the lab revealed the homodimer association constants ranged from 0.7–1.1 M^{-1} and the heterodimer was almost two orders of magnitude more stable (K_a of 50 M^{-1}) in CD_2Cl_2.[34] Zimmerman and coworkers later performed an incredible service to this field by providing a survey of hundreds of such simple hydrogen bonded dimers.[35] These studies revealed a similar range for association constants in simple DA-AD hydrogen bonded systems in nonpolar solvents, underscoring the magnitude of association constants of upwards of 500 M^{-1} in the compounds of class **1** (*cf.* Table 3).

‡This course also featured additional lectures by one of the guest editors, Pablo Ballester, who substituted for Prof. Rebek when the taxes of teaching and travelling took too large a toll.

Results and discussion

Synthesis

To modify the electron distribution on the six-membered PN heterocyclic core effectively, atomic coefficients analysis of the frontier molecular orbitals (FMOs) was performed on the unsubstituted PN-skeleton (Fig. 2). The results show that carbon 3, on which the R^1-substituted aryl ring resides, has a higher contribution to the LUMO. In contrast, carbon 6 shows a higher contribution to the HOMO occupancy levels. These results suggest that an EDG on C6 would efficiently raise the energy level of the HOMO, while an EWG on C3 would readily lower the energy level of the LUMO.[36–38] This should lead to a typical donor–acceptor (D–A) system and thus will likely push emission to longer wavelengths, in analogy to the well-established design principles for carbostyril fluorophore development to further red-shift emission and increase the quantum yield.[10,13]

To test this hypothesis, a family of PN-heterocycles containing a variety of EWGs and EDGs on carbons 3 and 6 (**1a–1p**) was synthesized according to Scheme 1. Typically, readily accessible 2-iodoaniline derivatives **2**[39] were alkynylated with terminal arylacetylenes **3** *via* Sonogashira cross-coupling to form the requisite arylethynylaniline precursors **4**. Because of purification difficulties, compounds **4i–4l** were prepared by an alternate route. Starting from known aniline **5**,[40] desilylation and Sonogashira cross-coupling of the crude product with the respective aryl halide afforded the remaining arylethynylanilines **4i–4l**. Finally, precursors **4** were treated with $P(OPh)_3$ in pyridine for 12–48 h at 110 °C and subsequently hydrolyzed to furnish PN-heterocycles **1**. Yields of **1** range from 26–61%, and recrystallization from $CHCl_3$ and hexanes gave analytically pure product. Examination of the ^1H and ^{31}P NMR spectra of **1** in $CDCl_3$ revealed a few interesting characteristics of this class of heterocycles. Specifically, the proton signal for the hydrogen attached to C4 shows up as a doublet with a relatively large coupling constant of *ca.* 40 Hz due to splitting by the phosphonamidate P. Additionally, the N–H proton shifts appear as a broad singlet within the 7–10 ppm range and the ^{31}P shifts show up as a doublet (J = *ca.* 40 Hz) around 9–12 ppm; however, both signals shift somewhat as a function of concen-

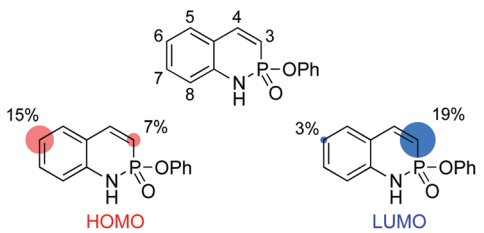

Fig. 2 Carbon atomic contributions (calculated at B3LYP/6-31 g(d) level of theory) to the HOMO (left) and LUMO (right) electron densities of the unsubstituted PN-heterocycle core and numbering order for core carbons (middle). Atomic contributions are shown only for the readily functionalizable positions.

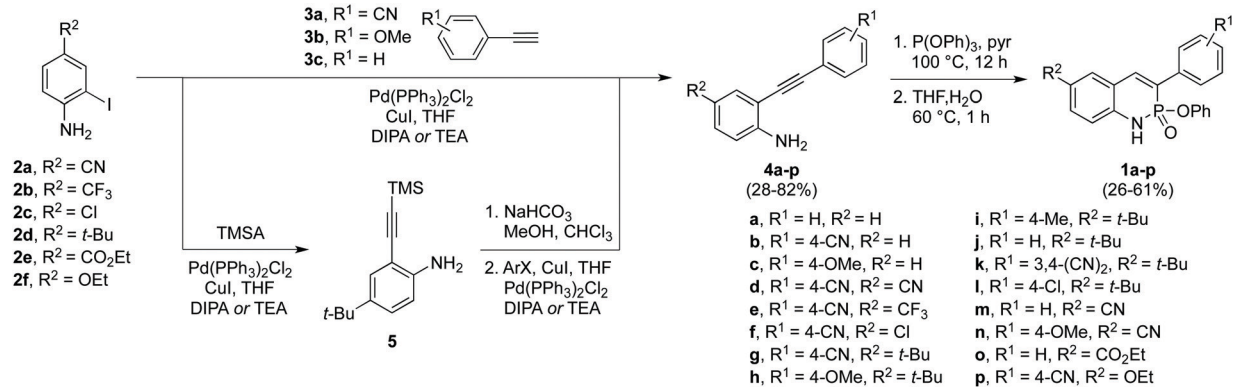

Scheme 1 General synthetic pathway for preparation of disubstituted PN heterocycles **1a–1p**.

tration due to dimer formation in solution (*vide infra*; see ESI†).

Photophysical properties

With compounds **1a–1o** in hand, their photophysical properties were measured and the results are summarized in Table 1. Based on the theoretical results above, one could expect that either withdrawing R^1 substituents or donating R^2 substituents would induce a red shift in the emission. In general, this hypothesis is corroborated by the absorption and emission properties of the designed families, where one group contains a withdrawing cyano group for R^1 and a variety of EDGs and EWGs for R^2 (Fig. 3a and S4a†), and the other contains a donating *tert*-butyl group for R^2 with a range of EDGs and EWGs for R^1 (Fig. 3b and S4b†). It is worth noting that the fluorescence behavior of the phosphaquinolinones is similar to that of analogously substituted carbostyrils, though somewhat red-shifted. For example, 3-phenylcarbostyril absorbs at 345 nm, and emits at 410 nm, whereas **1a** absorbs at 354 nm and emits at 427 nm.[13]

In these two families, clear trends can be drawn between substituent group electronic character and the emission energy (Fig. 3c), which are supported by further functional group orientations studied on both positions (Fig. S4†). Though there is a linear trend between emission energies and the Hammett σ_{para} parameter[41] on R^1 (red line in Fig. 3c, R^2 = 0.975), the trend between emission energy and Hammett parameter on R^2, though present, is not as clear (blue line in Fig. 3c, R^2 = 0.674). These trends are exemplified when comparing emission wavelengths of **1k** (477 nm) and **1h** (421 nm) (Table 1), which contain a withdrawing 3,4-$(CN)_2$ moiety and a donating 4-OMe group, respectively.

To gain insight into these trends and correlate them to substituent effects on the electronic structures, density functional theory (DFT) calculations were performed on **1a–1p**. Based on this data, there is indeed a substituent effect from groups on R^1. The HOMO levels trend upwards with more donating groups, going from −6.89 (**1d**) to −6.43 eV (**1g**) (Table 2, Fig. 4a), and the LUMO goes from −2.62 (**1k**) to −1.70 eV (**1h**) (Table 2, Fig. 4b) with more withdrawing groups on R^1. As

Table 1 Photophysical properties for PN-heterocycles **1**[a]

cmpd	R^1	R^2	λ_{abs} (nm)	λ_{em} (nm)	Stokes shift (nm/cm)	ε (cm^{-1} M^{-1})	ϕ^b (%)	τ^c (ns)
1a	H	H	335	417	82/5869	13 000	8	0.2
1b	4-CN	H	348	442	94/6112	22 000	11	0.3
1c	4-OMe	H	340	411	71/5080	17 000	7	0.2
1d	4-CN	CN	346	430	84/5646	12 000	18	0.5
1e	4-CN	CF_3	341	429	88/6015	20 000	11	0.3
1f	4-CN	Cl	358	450	92/5710	23 000	11	0.7
1g	4-CN	*t*-Bu	358	453	95/5858	22 000	11	0.5
1h	4-OMe	*t*-Bu	344	421	77/5316	16 000	6	0.3
1i	4-Me	*t*-Bu	343	424	81/5569	14 000	8	0.3
1j	H	*t*-Bu	343	430	87/5899	17 000	8	0.3
1k	3,4-$(CN)_2$	*t*-Bu	371	477	106/5989	19 000	41	1.9
1l	4-Cl	*t*-Bu	345	431	86/5784	19 000	8	0.4
1m	H	CN	337	410	73/5283	12 000	13	0.3
1n	4-OMe	CN	345	471	126/7754	15 000	28	0.7
1o	H	CO_2Et	335	411	76/5519	12 000	10	0.2
1p	4-CN	OEt	379	490	111/5977	25 000	24	2.4

[a] All measurements obtained at room temperature in $CHCl_3$. [b] Quantum yield measurements obtained with *ca.* 10^{-5} M solutions. [c] λ_{ex} = 344 nm; decay curves fitted to a monoexponential model.

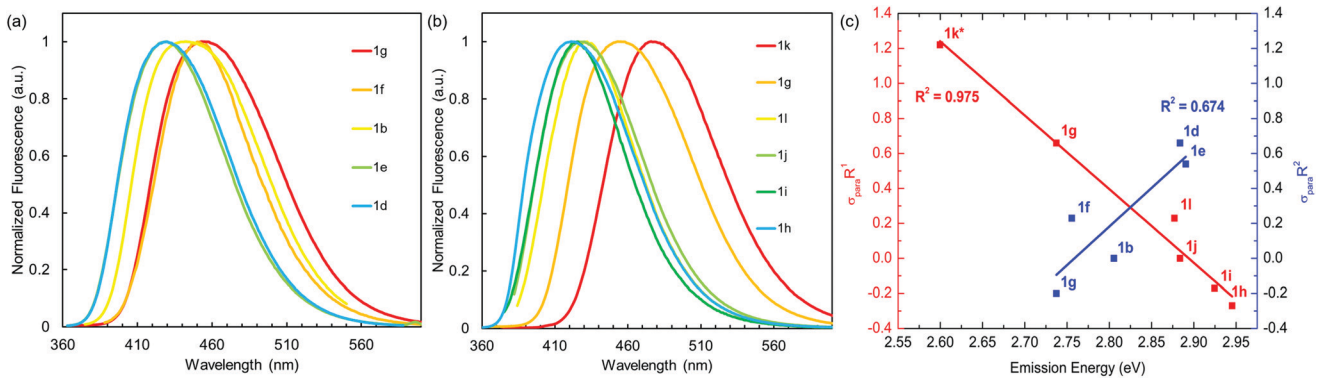

Fig. 3 Emission spectra of (a) heterocycles **1b**, **1d–1g** and (b) heterocycles **1g–1l** as well as (c) plot of trend between substituent electronic properties and emission energies of **1**. The σ value of **1k** was approximated by addition of the σ_{meta} and σ_{para} values of the two nitrile groups. All experimental values collected in $CHCl_3$.

Table 2 Orbital energy levels for **1a–1p** calculated at the PBE0/6-311G (d,p) level of theory

Cmpd	HOMO (eV)	LUMO (eV)	HOMO–LUMO gap (eV)
1a	−6.40	−1.84	4.56
1b	−6.59	−2.28	4.31
1c	−6.08	−1.74	4.34
1d	−6.89	−2.50	4.39
1e	−6.83	−2.43	4.40
1f	−6.63	−2.41	4.22
1g	−6.43	−2.24	4.19
1h	−6.04	−1.70	4.34
1i	−6.22	−1.76	4.46
1j	−6.29	−1.81	4.48
1k	−6.58	−2.62	3.96
1l	−6.34	−1.91	4.43
1m	−6.69	−2.13	4.56
1n	−6.29	−2.03	4.26
1o	−6.55	−1.96	4.59
1p	−6.16	−2.27	3.89

shown in Fig. 5, the FMOs of **1e–g** encompass the entire molecular systems, so the predominant transitions are $\pi \rightarrow \pi^*$ in nature.

TD-DFT was also performed to give a theoretical representation of the electronic transitions taking place (Fig. 5). For each heterocycle, the $S_0 \rightarrow S_1$ transition is dominated by the HOMO → LUMO transition, which is in good agreement with experimental absorption values (Table 1). The second longest wavelength absorption (*ca.* 300 nm) is predominantly composed of the HOMO−1 → LUMO transition and matches the experimental data for each heterocycle as well (Fig. S4†). In an attempt to better understand the electrochemical properties cyclic voltammetry (CV) measurements were collected for a subset of heterocycles **1** (Fig. S22†). While electrochemical gap values of *ca.* 4.0 eV could be determined, potential decomposition of the compounds upon measurement as well as constantly shifting magnitudes of the occurring redox events prevented accurate experimental determination of the HOMO and LUMO energy levels.

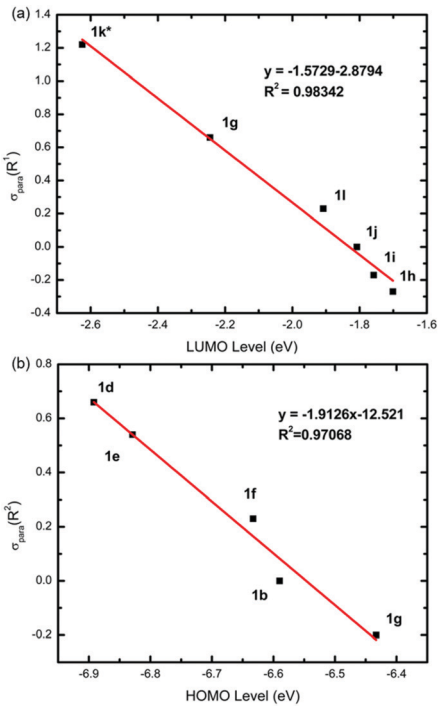

Fig. 4 (a) Calculated LUMO levels *vs.* Hammett parameter of R^1 substituents of R^2 = *t*-Bu heterocycles **1** and (b) calculated HOMO levels *vs.* Hammett parameter of R^2 substituents of R^1 = CN heterocycles **1**. Orbital energy levels calculated at the PBE0/6-311G(d,p) level of theory. The σ value of **1k** was approximated by addition of the σ_{meta} and σ_{para} values of the two nitrile groups.

Comparison of the computed HOMO–LUMO energy gaps of **1** with the experimental emission energies (Fig. 6a) showed that values are in very good agreement, such that the model should be able to predict emission energies accurately. To demonstrate this, we designed "optimized" heterocycle **1p** (R^1 = 4-CN and R^2 = OEt), as the –OEt group can donate relatively strongly with a Hammett σ_{para} parameter of −0.24 and thus should afford a dramatically red-shifted emission. The HOMO (−6.16 eV) and LUMO (−2.27 eV) levels were calculated,

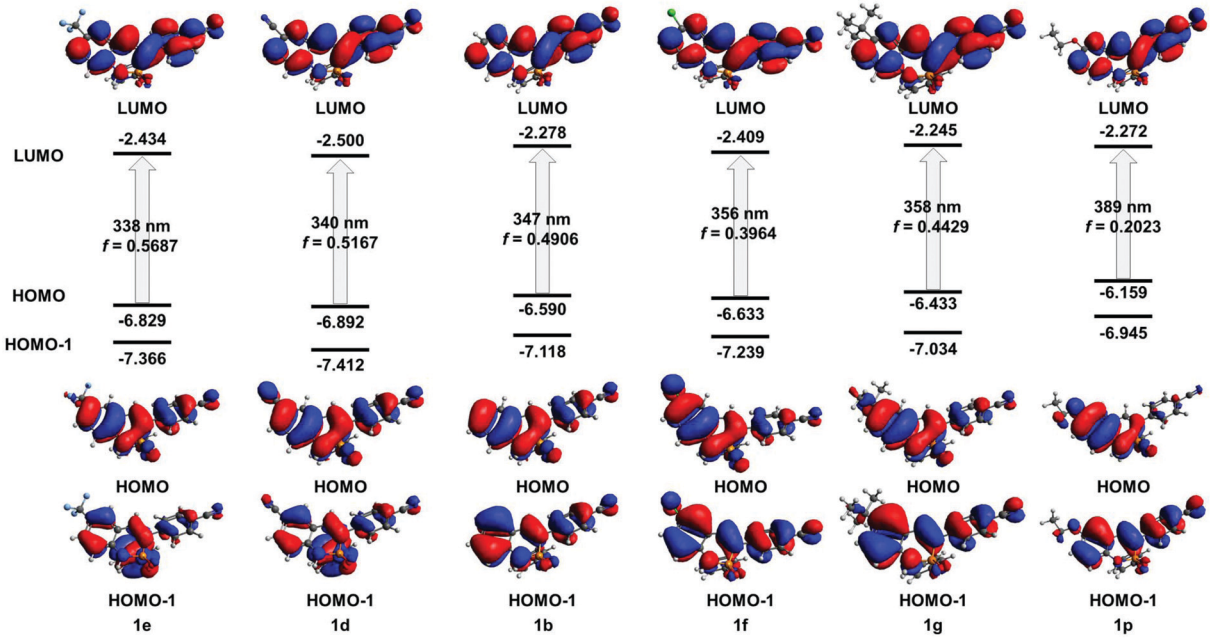

Fig. 5 Orientation of most dominant electronic transitions and the corresponding orbitals for heterocycles **1b**, **1d–1g**, and **1p**; orbital energies in eV.

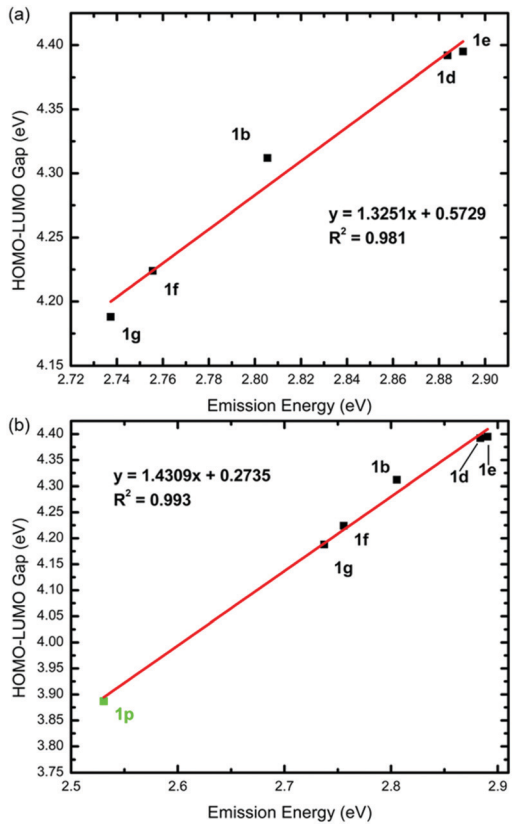

Fig. 6 Correlation between calculated HOMO–LUMO energy gap levels *versus* experimental emission energies of (a) heterocycles **1b**, **1d–1g**, and (b) heterocycles **1b**, **1d–1g**, and **1p**.

yielding a HOMO–LUMO gap of 3.89 eV. Based on this value, and the trend given by the related heterocycles in Fig. 6a, the predicted emission energy value for **1p** is 2.50 eV (496 nm). To validate this prediction, **1p** was prepared in a similar fashion shown in Scheme 1 starting from iodoaniline **2f**. Subsequent photophysical characterization showed λ_{em} = 490 nm (λ_{abs} = 379 nm, ε = 25 000 M^{-1} cm^{-1}, ϕ = 24%, and τ = 2.4 ns). This is in excellent agreement with the predicted value (Fig. 6b), showing that the trend seen between emission and HOMO–LUMO energy gaps can be empirically used to predict the emission of this PN scaffold.

Dimer formation in solution

In addition to studying the structure–property relationships between substituents and the photophysical aspects of heterocycles **1**, we have also investigated the effects that these substitutions have on the dimerization strengths. Based on the previously reported value of 130 M^{-1} for **1b**,[31] and the role of the N–H hydrogen acting as the dominant hydrogen bonding unit, further polarization of the N–H bond should lead to even higher dimer strengths. Logic would follow that including various withdrawing groups upon the scaffold should lead to this enhanced polarization. With these principles in mind, the dimer strengths of heterocycles **1** with a variety of EWGs and EDGs appended were studied using variable concentration (VC) NMR experiments in H_2O-saturated $CDCl_3$, with the results listed in Table 3 (see Experimental section in ESI† for measurement details).

Once the data is organized into families sharing either a similar R^1 or R^2 group, the resultant two LFERs (Fig. 7a and b) show that more withdrawing groups upon either R^1 or R^2 lead to stronger dimer formation. Notably, the strength changes

Table 3 Dimerization constants (M^{-1}) of heterocycles **1** in H_2O-saturated $CDCl_3$ [a]

Entry	K_{dim}	Entry	K_{dim}
1a	62[b]	**1i**	38[b]
1b	130[c]	**1j**	44
1c	56	**1k**	—[d]
1d	—[d]	**1l**	—[d]
1e	293	**1m**	525
1f	—[d]	**1n**	—[d]
1g	70	**1o**	200
1h	36	**1p**	87

[a] All values ±10%. [b] ^{31}P NMR signal tracked concomitantly to give 65 M^{-1} for **1a** and 41 M^{-1} for **1i**, which agree well with the respective ^{1}H NMR values. [c] Previously reported in ref. 31. [d] Not measurable due to low solubility.

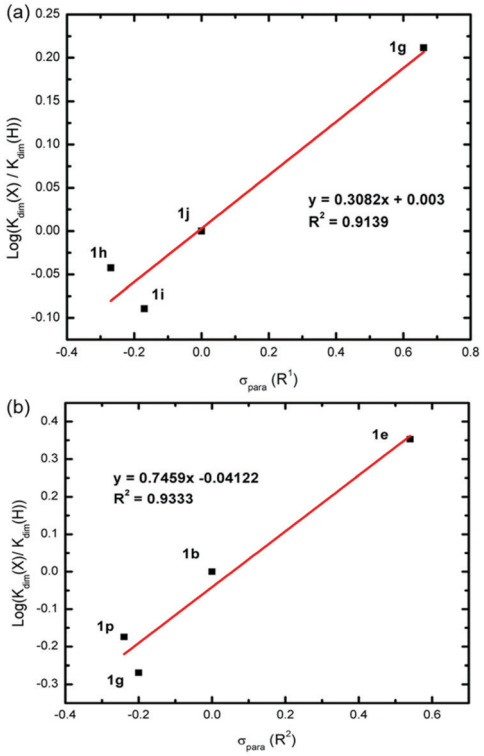

Fig. 7 Positive trends between EWG on (a) R^1 and (b) R^2 with dimerization constants of **1**.

over 2.5 times as much with varying σ_{para} of the substituents on R^2 than it does for R^1 based on the slope of the trends, showing the R^2 position is more sensitive to influencing dimerization strength. This is best illustrated when comparing heterocycles **1b** and **1m**, which have a nitrile group in place of R^1 and R^2, respectively. Installing the cyano unit on the *para* position with respect to the N–H in **1m** likely causes a much greater polarization, leading to a vastly increased dimer strength of 525 M^{-1}. To our knowledge, this value exceeds any previously reported for similar two-component hydrogen-bonded dimer systems.[35]

To better understand the nature of this dimerization, ΔG values (ΔG_{calc}) were calculated and compared to experimental values (ΔG_{exp}) (Table 4). While the computed ΔG_{calc} values are very similar to the ΔG_{exp} values, the trends do not track in all cases. The ΔG_{exp} values are incredibly close to each other, making it difficult to precisely match computationally. Interestingly, the gas phase free energies matched experimental trends more closely (Table S17†), with several additional computational methods explored (see ESI†).

Table 4 ΔG_{calc} and ΔG_{exp} values of heterocycles **1** [a]

Entry	ΔG_{calc}	ΔG_{exp}
1g	−3.1	−2.5
1b	−2.1	−2.9
1e	−2.4	−3.4
1p	−1.6	−2.6
1j	−2.2	−2.2
1m	−2.7	−3.7
1a	−3.3	−2.4
1o [b]	−2.6	−3.1
1h	−2.5	−2.1
1c	−2.5	−2.4

[a] Optimization performed with PBE/6-31G(d); single points done at WB97X/6-311++G(2df,p). Solvation corrections done in $CHCl_3$ at PBE/6-31+G(d,p)/SMD. [b] CO_2Me ester substituent was used in place of the CO_2Et ester, which share very similar Hammett parameters, to lessen the computational load.

The models also show that the most stable dimer is always formed between one *R* and one *S* enantiomer because of stereoelectronic effects between phenoxy groups on each phosphorus center, corroborating the crystal packing structures reported in this paper (Fig. 8, S1–S3 and S6†) as well as those of previous studies.[31,32] In the heterodimer, the phenoxy oxygen lone pairs can donate into the P–O σ* and P–N σ* orbitals, which are stabilizing interactions (Fig. 8a). In the homodimer only one phenoxy oxygen can be in the correct orientation to donate into the P–O σ* and P–N σ* orbitals; the other one is rotated to avoid steric collision between the phenoxy groups (Fig. 8b). The rotated phenoxy group donates into the P–O σ* and P–C σ* orbitals, which are still stabilizing interactions, but less stabilizing than the lone pairs donating into the P–O σ* and P–N σ* orbitals. When the phenoxy groups are replaced with methoxy groups, there is no appreciable energy difference between the homodimer and heterodimer.

Using a multiple linear regression model in R,[42–44] the ΔG_{exp} values were plotted as a function of the σ_{para} values of both the R^1 and R^2 groups, giving a method for the prediction of the strength of a dimer with any combination of R^1 and R^2 substituent groups on any similar phosphaquinolinone molecule (eqn (1)). Two values were excluded from the initial model and used as a validation set to verify the predictive ability of the model (Fig. 9, Table S18†).§

$$\Delta G_{Pred} = -2.53989 - 0.42865(\sigma_{para}R^1) - 1.42686(\sigma_{para}R^2) \quad (1)$$

§ ΔG_{exp} of dimer formation as a function of Hammett parameters of both R^1 and R^2 substituent groups; adjusted R^2 = 0.91 and *p*-value = 0.00026.

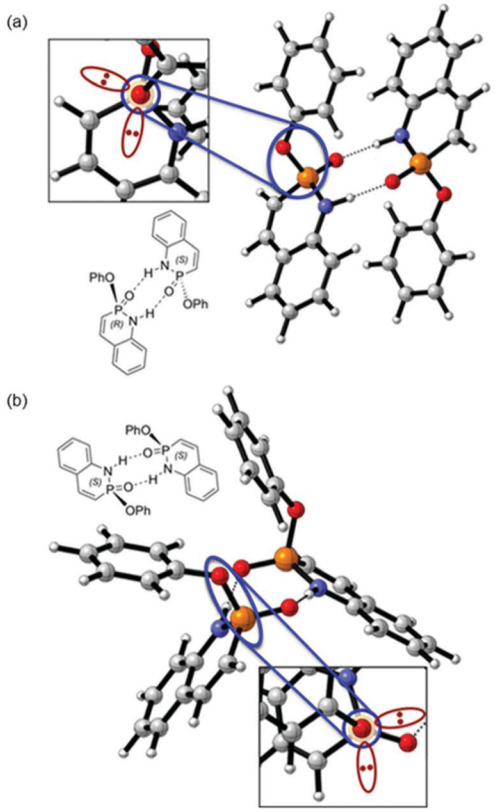

Fig. 8 Schematic examples of (a) orbital overlap within monomer units in the R–S heterodimer structure and (b) poor alignment between orbitals within each monomer in the S–S homodimer structure, where the phenoxy oxygen lone pairs are represented in red and align with the P–O σ* and P–N σ* orbitals and the P–O σ* and P–C σ* orbitals, respectively.

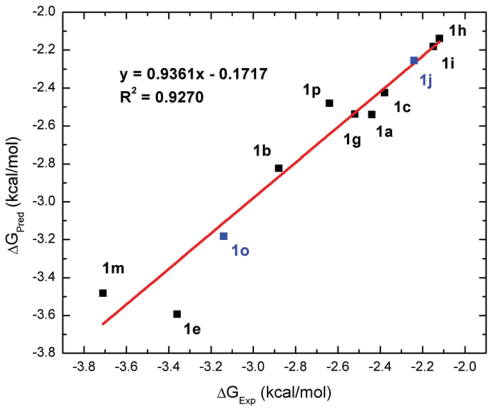

Fig. 9 ΔG_{exp} values *versus* ΔG_{pred}. Blue data points were omitted from the initial model, and tested as a validation set of data, showing a good correlation to the model.

Dimer formation in solid state

In an attempt to corroborate solution state data for the strength of the hydrogen bonding interactions between **1** monomers with hydrogen bonding in the solid state, single crystals were grown by vapor diffusion of pentane into concentrated $CHCl_3$ solutions of **1b**, **1c**, **1e**, **1g**, and **1m** (Fig. 10 and S1–3†). In the solid-state structures, heterocycles **1b**, **1c**, and **1m** crystalize as the previously observed[31,32] *meso*-dimers discussed above (Fig. 10a). Interestingly, both **1e** and **1g** instead form a staggered, repeating hydrogen bonding system, where the N–H and P═O moiety of each monomer coordinates with a different heterocycle, forming a continuous zigzag chain (Fig. 10b). This alternative packing mode is likely due to steric interactions caused by the *t*-Bu and the trifluoromethyl groups on **1e** and **1g**, respectively, thus likely inhibiting formation of the usual dimer structure in the solid state.

Regardless of the molecular packing, which can be influenced by various factors that do not affect the solution state, each structure shows the characteristic N···O interactions of the phosphonamidate scaffold, distances that are summarized in Table 5. Compared to the respective solution state dimerization strength (Fig. 11), the data is suggestive of a close relationship between the two, where the congeners with the higher

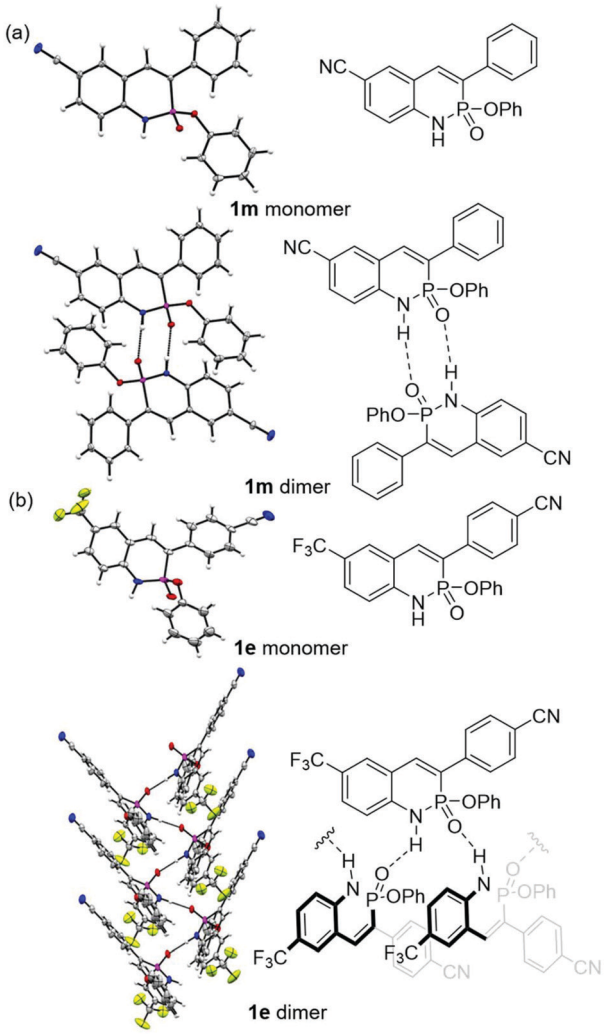

Fig. 10 Solid state structures of (a) the monomer and dimer of **1m** and (b) the monomer and staggered hydrogen bonding network of **1e**.

Table 5 Solid state N···O distances of selected heterocycles **1**

Entry	N···O distance (Å)
1b	2.809(2)
1c	2.821(11)
1e	2.807(4)
1g	2.815(2)
1m	2.768(2)

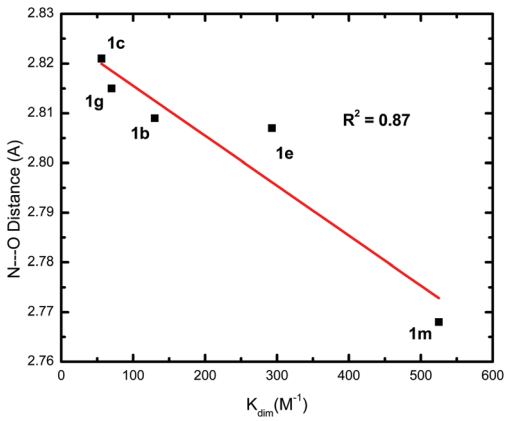

Fig. 11 Solid state N···O distances plotted against solution state K_{dim} values measured in $CDCl_3$.

K_{dim} values indeed have shortened N···O distances. Though there exist a multitude of factors that influence the solid state and the solution state separately, this relationship may hint toward potential guided design of these molecules as subunits in larger hydrogen-bonded systems.

Conclusions

In summary, we have reported an expedited synthesis of a unique PN heterocyclic scaffold, as well as studied the effects of substitution upon two sites. Specifically, the relationships between calculated HOMO and LUMO energy levels of each derivative and the experimental emission characteristics were developed. The design principles learned from this correlation were then employed to synthesize another derivative with further red-shifted emission. In addition, we elucidated the nature of the very strong *meso*-dimers observed for these heterocycles by characterizing their solution state strengths as a function of substituent groups, comparing them with computed values, and correlating their solid-state N···O distances. The work described above addresses deficiencies in the knowledge about this new scaffold and provides both experimental and computational evidence towards current hypotheses surrounding them. This work will assist future guided design of this unique heterocycle for applications in chemosensing, anion sensing, and supramolecular materials, which we believe are worth additional exploration by us and hopefully others given the strong, complementary hydrogen bonding and emerging anion binding selectivity.[45]

Conflicts of interest

There are no conflicts to declare.

Acknowledgements

We thank the National Science Foundation (INFEWS CHE-1607214 to MMH/DWJ and CHE-1352663 to PHYC) for support of the research. Mass spectrometry capabilities in the CAMCOR facility are supported by the NSF (CHE-1625529). This work was supported by the Bradshaw and Holzapfel Research Professorship in Transformational Science and Mathematics to DWJ. PHYC is the Bert and Emelyn Christensen professor of OSU and gratefully acknowledges financial support from the Vicki & Patrick F. Stone family.

Notes and references

1 R. S. Becker, S. Chakravorti, C. A. Gartner and M. de Graca Miguel, *J. Chem. Soc., Faraday Trans.*, 1993, **89**, 1007.
2 G. A. Reynolds and K. H. Drexhage, *Opt. Commun.*, 1975, **13**, 222.
3 V. F. Traven, A. V. Manaev, A. Y. Bochkov, T. A. Chibisova and I. V. Ivanov, *Russ. Chem. Bull.*, 2012, **61**, 1342.
4 F. G. Medina, J. G. Marrero, M. Macías-Alonso, M. C. González, I. Córdova-Guerrero, A. G. Teissier García and S. Osegueda-Robles, *Nat. Prod. Rep.*, 2015, **32**, 1472.
5 V. F. Traven and A. Y. Bochkov, *Heterocycl. Commun.*, 2013, **19**, 219.
6 S.-L. Pan, K. Li, L.-L. Li, M.-Y. Li, L. Shi, Y.-H. Liu and X.-Q. Yu, *Chem. Commun.*, 2018, **54**, 4955.
7 M. A. Salem, M. H. Helal, M. A. Gouda, Y. A. Ammar, M. S. A. El-Gaby and S. Y. Abbas, *Synth. Commun.*, 2018, **48**, 1534.
8 M. B. de Macedo, R. Kimmel, D. Urankar, M. Gazvoda, A. Peixoto, F. Cools, E. Torfs, L. Verschaeve, E. S. Lima, A. Lyčka, D. Milićević, A. Klásek, P. Cos, S. Kafka, J. Košmrlj and D. Cappoen, *Eur. J. Med. Chem.*, 2017, **138**, 491.
9 A. B. Ahvale, H. Prokopcová, J. Šefčovičová, W. Steinschifter, A. E. Täubl, G. Uray and W. Stadlbauer, *Eur. J. Org. Chem.*, 2008, 563.
10 G. Uray, K. S. Niederreiter, F. Belaj and W. M. F. Fabian, *Helv. Chim. Acta*, 1999, **82**, 1408.
11 G. A. Strohmeier, W. M. F. Fabian and G. Uray, *Helv. Chim. Acta*, 2004, **87**, 215.
12 G. C. Enoua, G. Lahm, G. Uray and W. Stadlbauer, *J. Heterocycl. Chem.*, 2014, **51**, E263.
13 W. M. F. Fabian, K. S. Niederreiter, G. Uray and W. Stadlbauer, *J. Mol. Struct.*, 1999, **477**, 209.
14 T. Tashima, *Bioorg. Med. Chem. Lett.*, 2015, **25**, 3415.

15 J. R. Casley-Smith, R. G. Morgan and N. B. Piller, *N. Engl. J. Med.*, 1993, **329**, 1158.
16 C. X. Jiao, C. G. Niu, L. X. Chen, G. L. Shen and R. Q. Yu, *Anal. Bioanal. Chem.*, 2003, **376**, 392.
17 R. Vekariya and H. Patel, *Synth. Commun.*, 2014, **44**, 2756.
18 B. D. Wagner, *Molecules*, 2009, **14**, 210.
19 M. J. S. Dewar and V. P. Kubba, *J. Am. Chem. Soc.*, 1960, **82**, 5685.
20 I. G. M. Campbell and J. K. Way, *J. Chem. Soc.*, 1960, 5034.
21 W. Tang and Y.-X. Ding, *J. Org. Chem.*, 2006, **71**, 8489.
22 W. Tang, Y. Ding and Y.-X. Ding, *Tetrahedron*, 2008, **64**, 10507.
23 J. Yan, Q. Li, J. A. Boutin, M. P. Renard, Y. Ding, X. Hao, W. Zhao and M. Wang, *Acta Pharmacol. Sin.*, 2008, **29**, 752.
24 S. Park, B. Seo, S. Shin, J.-Y. Son and P. H. Lee, *Chem. Commun.*, 2013, **49**, 8671.
25 D. Zhao, C. Nimphius, M. Lindale and F. Glorius, *Org. Lett.*, 2013, **15**, 4504.
26 Z.-Q. Lin, W.-Z. Wang, S.-B. Yan and W.-L. Duan, *Angew. Chem., Int. Ed.*, 2015, **54**, 6265.
27 L. Liu, A.-A. Zhang, Y. Wang, F. Zhang, Z. Zuo, W.-X. Zhao, C.-L. Feng and W. Ma, *Org. Lett.*, 2015, **17**, 2046.
28 Y. Sun and N. Cramer, *Angew. Chem., Int. Ed.*, 2017, **56**, 364.
29 Y.-N. Ma, X. Zhang and S.-D. Yang, *Chem. – Eur. J.*, 2017, **23**, 3007.
30 Z. Wang, B. S. Gelfand and T. Baumgartner, *Angew. Chem., Int. Ed.*, 2016, **55**, 3481.
31 C. L. Vonnegut, A. M. Shonkwiler, M. M. Khalifa, L. N. Zakharov, D. W. Johnson and M. M. Haley, *Angew. Chem., Int. Ed.*, 2015, **54**, 13318.
32 N. A. Takaesu, E. Ohta, L. N. Zakharov, D. W. Johnson and M. M. Haley, *Organometallics*, 2017, **36**, 2491.
33 T. Martín, U. Obst and J. Rebek Jr., *Science*, 1998, **281**, 1842.
34 F. Hof, *Self-Assembled Tetrameric Capsules*, *PhD Thesis*, The Scripps Research Institute, 2003.
35 See the detailed ESI in: J. R. Quinn, S. C. Zimmerman, J. E. Del Bene and I. Shavitt, *J. Am. Chem. Soc.*, 2007, **129**, 934.
36 E. Kim, M. Koh, B. J. Lim and S. B. Park, *J. Am. Chem. Soc.*, 2011, **133**, 6642.
37 X. Liu, Q. Qiao, W. Tian, W. Liu, J. Chen, M. J. Lang and Z. Xu, *J. Am. Chem. Soc.*, 2016, **138**, 6960.
38 X. Liu, Z. Xu and J. M. Cole, *J. Phys. Chem. C*, 2013, **117**, 16584.
39 D. B. Kimball, T. J. R. Weakley and M. M. Haley, *J. Org. Chem.*, 2002, **67**, 6395.
40 C. N. Carroll, O. B. Berryman, C. A. Johnson, L. N. Zakharov, M. M. Haley and D. W. Johnson, *Chem. Commun.*, 2009, 2520.
41 C. Hansch, A. Leo and R. W. Taft, *Chem. Rev.*, 1991, **91**, 165.
42 R Core Team (2017). R: A language and environment for statistical computing. R Foundation for Statistical Computing, Vienna, Austria. URL https://www.R-project.org/.
43 H. Wickham, *ggplot2: Elegant Graphics for Data Analysis*, Springer-Verlag, New York, 2009.
44 K. Slowikowski, *ggrepel: Repulsive Text and Label Geoms for 'ggplot2'. R package version 0.7.0*, 2017, https://CRAN.R-project.org/package=ggrepel.
45 C.-L. Deng, J. P. Bard, J. A. Lohrman, J. E. Barker, L. N. Zakharov, D. W. Johnson and M. M. Haley, *Angew. Chem., Int. Ed.*, 2019, **58**, 3934.